NANO MICRO small

Graphene

Growing Suspended Graphene on C_{60} Molecules

*Jiong Lu, Yi Zheng, Anastassia Sorkin, and Kian Ping Loh**

1. Introduction

The remarkable electronic properties of graphene with its tunable electron density and high carrier mobility, renders it highly attractive for application in electronic devices.[1–4] However, the two dimensional and ultrathin nature of graphene makes its electronic properties highly susceptible to the influence of the substrate. Strong interfacial electronic coupling of graphene to the substrate distorts its linear π-bands near the Fermi energy and reduces the mobility of the carriers.[5,6] For example, ultrahigh mobility is only realized on freestanding graphene sheets that are uncoupled from the ionized impurity scattering effect of the substrate.[7,8] In addition, compressive stress arising from lattice mismatch between graphene and the substrate results in strain-relief corrugated features like the Moiré superlattice, which possesses a complex energy landscape that distorts the carrier dynamics on flat graphene. Introducing foreign atoms or molecules into the interface between graphene and substrate, so called intercalation, is a potential strategy to uncouple the epitaxial graphene from the substrate, flatten it and restore its massless Dirac fermions.[5,6,9] Although graphite intercalation compound has been studied extensively,[10–13] insights into the intercalation chemistry that occurs between epitaxial graphene and the substrate is only emerging recently.[14] Alternatively, it is interesting to consider the growth of suspended graphene directly over molecular precursors pre-anchored on metal surfaces so that quasi-freestanding graphene can be formed on top of those buried species without pinning to the metal substrate. The bending rigidity of graphene and in-plane strain can depin the graphene from the substrates once it grows over these molecules.[15]

To this end, we made the unique discovery that C_{60} molecules absorbed on Ru metal surface can at once act as growth precursors to graphene as well as suspension struts for the growing graphene sheet. The highly isotropic structures of C_{60} molecules with its high degree of internal freedom allow the molecules to adopt a diverse range of adsorption configurations on metal substrate, particularly at elevated temperature.[16,17] This gives rise to an unusually wide decomposition window for C_{60} which overlaps with other dynamical process like recrystallization. With careful control, we are able to prepare suspended graphene on immobilized C_{60} molecules. Most interestingly, the buried C_{60} molecules could be further decomposed to generate another layer of graphene and eventually form the bilayer graphene. The salient features of the whole process are illustrated in **Figure 1**.

2. Results and Discussion

Previous studies have shown that C_{60} molecules can be intercalated between as-grown graphene layer and nickel or iridium substrates.[13,18] However, there has been no report of molecular intercalation of epitaxial graphene on strongly interacting substrate such as ruthenium. High energy barriers have to be overcome when C_{60}-metal covalent interaction substitutes for the strong graphene–metal bonding. Since the binding energy of C_{60} on Ru is high, it is interesting to consider a reversed approach by growing the graphene directly on pre-assembled C_{60} layer. The strategy we applied is to begin with a closed-packed C_{60} molecular network on the surface. The assembly of C_{60} on Ru(0001) after annealing at 450 K produces a highly-ordered hexagonal matrix as shown in **Figure 2**a-b. Magnified STM images (Figure 2c) reveal that the C_{60} molecules show a uniform 3-fold symmetrical clover-pattern, which can be traced to the adsorption configuration of C_{60} with a six-carbon ring facing up (indicated in the top right panel of Figure 2c).[16] Upon annealing at 550 K, a disordered molecular network was observed (Figure 2d) and C_{60} molecules displayed either the dumbbell-shaped or clover-shaped configurations. The variation in molecular heights is due to the embedding of C_{60} molecules on the Ru substrate.[17] A dumbbell-shaped C_{60} is now imaged with a surface coverage ratio of approximately 50%. The dumbbell-shape is due to the orientation of the C_{60} molecules with a 6:6 bond (the C–C bond between two carbon hexagons) facing up as shown in Figure 2c.[19] Increasing the annealing temperature to 620 K, the C_{60} molecules aggregate into chain-like structures, as shown in Figure 2f.

The molecule–substrate interaction depends on adsorption configuration and interfacial distances.[20,21] Therefore, the possibilities of having more than one type of adsorption orientations led to different binding strengths between the C_{60} and Ru substrate, which subsequently translates to a wide window of decomposition temperature of C_{60} molecules on

Dr. J. Lu, Prof. K. P. Loh
Graphene Research Centre
National University of Singapore
6 Science Drive 2, Singapore 117546, Singapore
E-mail: chmlohkp@nus.edu.sg
Dr. J. Lu, Dr. Y. Zheng, Dr. A. Sorkin, Prof. K. P. Loh
Department of Chemistry
National University of Singapore
3 Science Drive 3, Singapore 117543, Singapore

DOI: 10.1002/smll.201201113

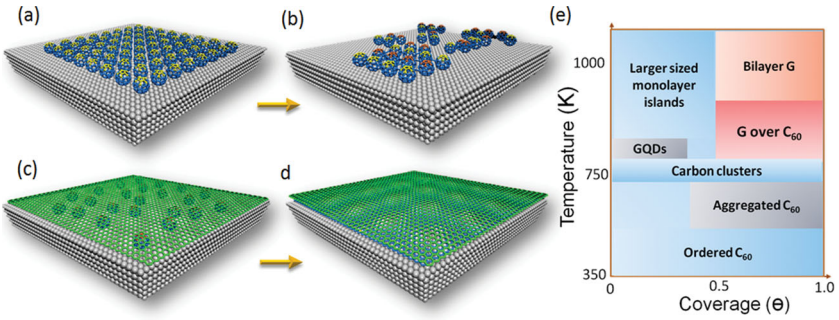

Figure 1. Illustration of the phase transitions of monolayer C_{60} on Ru(0001) at different annealing temperature. a) Self-assembled C_{60} molecules transform into highly-ordered monolayer C_{60} film. b) The aggregation of C_{60} molecules into "clover" or "dumbbell" configuration upon annealing at 500–620 K. c) Growth of suspended graphene on C_{60} molecules at 800–900 K. d) Transforming buried C_{60} into the second layer to form bilayer graphene at 900–1100 K. e) A scheme of coverage- and temperature-dependent phase diagram of C_{60} molecules on Ru(0001).

Ru. A further annealing step to 800-900 K decomposes C_{60} molecules partially. It is well-known that coalescence of C_{60} or C_{60}-derived fragments can self-organize into graphitic structures at high temperature.[17,22,23] Interestingly, we found that the fragments recrystallize into a floating graphene monolayer over the remaining C_{60} network on the Ru surface (Figure 1c and **Figure 3**). The float-growth can be rationalized by analyzing the bending and adhesion energies of graphene, as shown later. Upon annealing at 800 K for 5 min, ~30% of the C_{60} molecules decompose, while unconsumed C_{60} molecules are either embedded on Ru(0001) with an averaged intermolecular distance of ~1.4 nm or buried under growing graphene flakes with an averaged molecular space of ~2.2 nm. The observation of a lower density of buried C_{60} molecules under the suspended graphene suggests that these act as feedstock for the advancing graphene edges.

The in-situ growth of graphene over C_{60} was documented using HT-STM. After another 5 minutes, those regions marked by arrows in Figure 3a has extended in Figure 3b due to the continuous coalescence of C_{60} fragments into graphene, which is consistent with the observation of a slight decrease in the density of embedded C_{60} on Ru. The honeycomb lattice of graphene is visible in the regions without buried C_{60} molecules as shown in high-resolution STM image (inset of Figure 3h), which indicates the crystalline quality of the floating graphene sheet. Thermal annealing provides sufficient kinetic energy for the rearrangements of atoms, which is crucial for transforming the pentagons in C_{60} into prefect hexagons.

The buried C_{60} molecules can be imaged through graphene as a result of a strong bias-dependent spectroscopic contrast. The observed bias dependence of the corrugation for the buried C_{60} molecules is shown in Figure 3d. C_{60} molecules under graphene can be imaged with a brighter contrast at low sample bias (such as 60 meV), which is in good agreement with previous finding.[6] For a freestanding graphene monolayer, the symmetry group leads to a degeneracy of the π bands at the K points, where the Fermi level (E_F) intersects the π band and leads to a vanished density of states (DOS) at E_F but a sharp rise in the DOS above and below E_F.[4] The buried C_{60} molecules uncouple the interaction of graphene

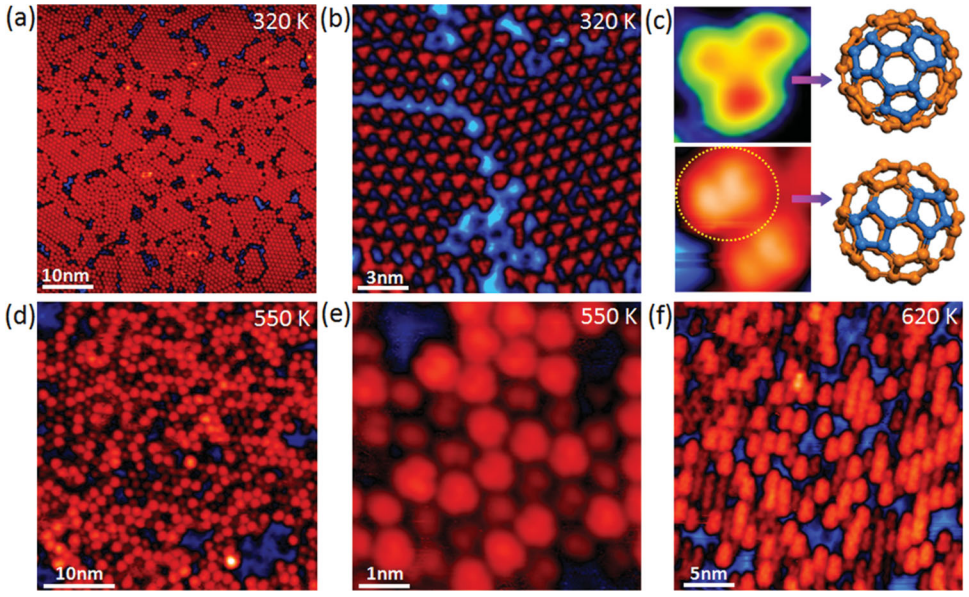

Figure 2. STM image of the evolution of 0.8–1 monolayer (ML) C_{60} film on Ru(0001) at different temperatures. a,b) Annealing the 0.8–1 ML C_{60} films at 320 K and magnified view shows C_{60} has an identical clover-shape adsorption configuration. c) The clover-shape (I) and dumbbell-shape C_{60} (II) and its corresponding molecular adsorption orientation. d,e) Initial states of the polymerization of C_{60} film occur at 550 K. f) Aggregation of C_{60} to form molecular chain-like structure at 620 K.

small 2012,
DOI: 10.1002/smll.201201113

NANO MICRO small

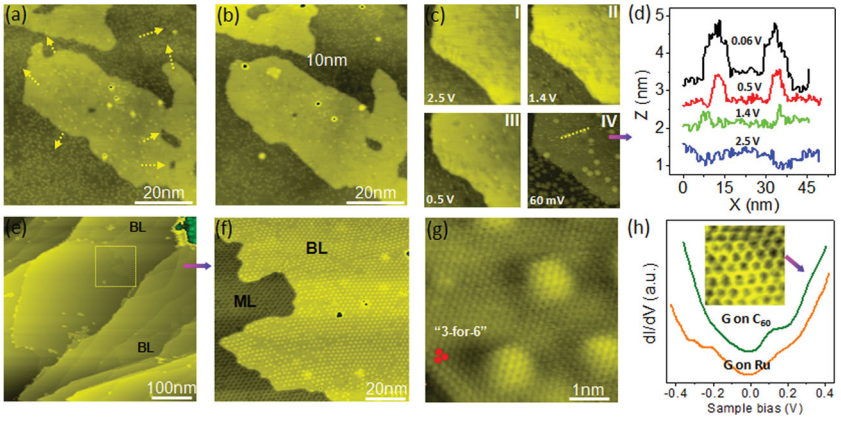

Figure 3. a) High-temperature STM images recorded at 800–850 K show graphene growing on C_{60} (arrows indicate the advancing growth front). b) The expansion in area of the graphene sheet shown earlier in (a) (taken at the same location as (a), after 5 minutes). c) Imaging of the buried C_{60} at different sample bias, and d) its bias-dependent corrugation due to tunneling from local DOS of the buried C_{60}. e,f) Growth of bilayer domain though the decomposition of interfacial C_{60} molecules at 900–1100 K. g) High-resolution STM image shows "3-for-6" triangular lattice in bilayer graphene. h) *dI/dV* curves for the epitaxial graphene grown on Ru(0001) and graphene grown on C_{60}; inset: the honeycomb lattice pattern of floating graphene (taken in the regions without underlying C_{60} molecules at room temperature).

with the Ru substrate and lift the Ru-induced *n*-doping. Thus the graphene suspended on C_{60} has freestanding-like character, which means there is negligible contribution of the graphene states to the overall tunneling current near the Fermi level. However at the regions with buried C_{60}, there will be higher local DOS due to the C_{60} and the corresponding local tunneling conductivity will increase, giving to an increased Z-corrugation (inset of Figure 3d) at these sites. Scanning tunneling spectroscopy (STS) (Figure 3h) performed on the floating graphene sheet indicate that its electronic property is modified by the buried C_{60} molecules. For epitaxial graphene grown on Ru(0001), the STS curve shows a dip at –0.3 eV corresponding to either a surface state of ruthenium substrate[24] or negative shift of Dirac points of graphene.[17,25] In contrast, a dip in the STS curve at +0.2 eV suggests the electronic decoupling of the graphene from ruthenium and p-type doping by the buried C_{60} molecules.

Thermal or electron-beam irradiation-induced coalescence of C_{60} inside SWCNT can transform the disconnected C_{60} molecular chain into an intertubular graphene, which is a type of channel-confined organization.[26,27] The parallel to the tube-within-a tube situation here is this: C_{60} molecules under the floating graphene are now sandwiched between the metal substrate and the first layer graphene, and should be transformable into a second layer graphene upon annealing. We verified this by a second annealing of the sample in the temperature range 900–1100 K, all the buried molecules decomposed into graphene as shown in Figure 3e-f. The bilayer graphene exhibits a so called "3-for-6" pattern (only three of the six carbon atoms in each hexagonal ring were imaged), which results from the top layer adopting an AB Bernal stacking with the bottom layer. Consequently, such commensurate stacking breaks the lattice symmetry of the top layer and gives rise to the triangular lattice pattern. In the case of incommensurate stacking, a hexagonal honeycomb lattice will be imaged instead.[28] However, the Moiré superlattice in the bilayer graphene appears to be disordered, which indicates the existence of misaligned domains (~30% of the total area).

The generation of floating graphene, as opposed to epitaxial growth of graphene on Ru substrate, depends sensitively on the surface coverage of C_{60} on Ru(0001). A minimum coverage of C_{60} of ~0.7–0.8 is required to allow the co-existence of both C_{60} and graphene phases (Figure 1). This will ensure that sufficient C_{60} fragments can recrystallise over pre-adsorbed C_{60} molecules instead of simply growing on top of the metal substrate. It is well-known that the immobilization of C_{60} on Ru is mediated by surface vacancy on Ru created after high-temperature annealing.[17] The subsequent molecular embedding will anchor the C_{60} on the surface before its decomposition and recrystallization. Therefore, the advancing graphene sheet has to climb over these embedded C_{60}. The subsequent molecular embedding will anchor the C_{60} on the surface before its decomposition and recrystallization. The bending rigidity of graphene dictates that there must be sufficient length scale for graphene-substrate adhesion to offset the elastic strain, otherwise it will be depinned from the substrate and suspend over the C_{60} as a flat sheet. If we consider the average distance between two buried C_{60} molecules to be X nm, a bending dominated regime occurs when X exceeds a certain threshold value such that adhesion energy of the graphene sheet on Ru is larger than its bending energies over the C_{60} molecules. At length scale smaller than this threshold distance, the bending rigidity and in-plane strain will depin the graphene sheet from the substrate. A statistical analysis of the inter-particle distance of the buried C_{60} molecules and theoretical estimation of the bending energy versus adhesive energy of graphene explains why the graphene prefers to depin from the substrate. In the case of the suspended graphene, we observed that the largest separation between two buried C_{60} is limited to 4 nm, with an average value of 2.5 nm as shown in **Figure 4**c. Quantitative analysis of the energetics in this system provides an insight into why suspension of the graphene sheet over the C_{60} molecules is favored over a conformal bending over it and attachment on substrate. The graphene–ruthenium adhesion energy (denoted as E_{pin}) can be calculated from the equation one (1),[15] where Υ_s is the coupling-constant strength of graphene grown on Ru(0001).

$$E_{pin} = \gamma_s \int d^2 x \qquad (1)$$

The coupling-constant Υ_s is calculated to be 8.6 meV/Å based on the total binding energy of graphene-Ru (–6.7 eV) per Moiré unit cell.[29] The bending energy of graphene membrane attached to the substrate scales as

DOI: 10.1002/smll.201201113

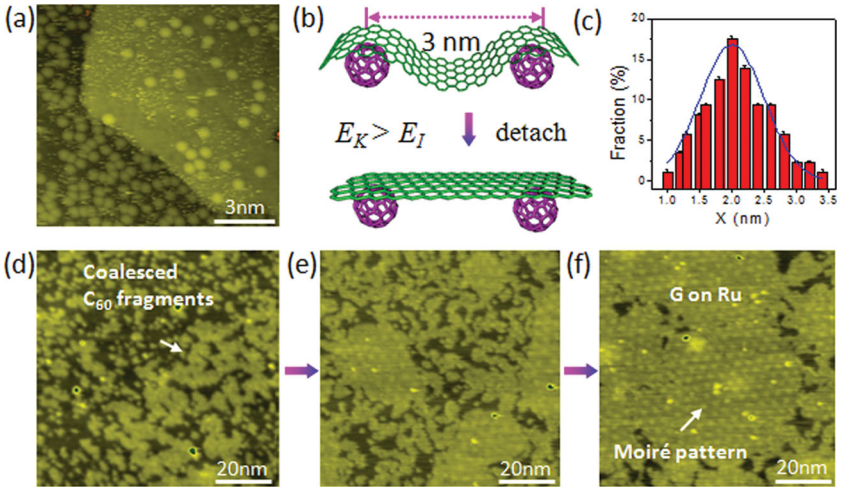

Figure 4. a) STM image of suspended graphene. b) Illustration of the detaching of graphene, depending on the distance between two adjacent C_{60} molecules. c) Histogram of experimentally observed distances between two buried C_{60} molecules, derived from various STM images (X: centre-to-centre distance between two adjacent C_{60} molecules). d–f) Series of STM images (taken at 800-850 K) of coalescence of C_{60} fragments into decoupled graphene on Ru(0001) with a low coverage (0.5 monolayer C_{60}).

$$E_K \sim \kappa \frac{h^2}{L^2} \quad (2)$$

where h is the height fluctuation over a length scale L and the bending rigidity of graphene κ is given by ≈ 1 eV.[30] For a graphene strip that is 3 nm long and 1 nm wide, its bending energy will be 2 eV when it sits on top of two 3 nm-separated C_{60} molecules immobilized on Ru. The interaction energy of graphene with the Ru substrate in this configuration is only –1.83 eV,[15] calculated from the sum of adhesion energy (E_{pin}) and van der Waals attraction between C_{60} and graphene.[31,32] Therefore, the depinning of the graphene from the substrate will be preferred since the adhesion energy is insufficient to offset the energy cost due to bending (Figure 4b). If the distance between two C_{60} is increased to 5 nm, the total interaction energy overwhelms the bending energy and thus results in the pinning of the graphene on Ru (see more details in Supporting Information). The threshold inter-particle C_{60}–C_{60} distance to depin graphene from Ru is found to be ~4.5 nm, which matches experimental results well.

The significance of this work suggests that growth of suspended graphene over nanostructures is possible if the nanostructures are of a certain aspect ratio and separated by a minimum distance that offset the adhesion energy on the substrate. In principle, a suspended graphene with a topographic superlattice which is defined by the periodicity of the nanopillars below can be prepared. Topographical corrugation on the suspended graphene can be created by corrugation of the intercalated particles below, affording a regular deformation of the lattice. This constitutes a new method to modify the energy landscape in graphene.

3. Conclusion

The phase transition of C_{60} film on Ru(0001) as a function of coverage and temperature has been carefully studied using STM. The temporal and spatial overlap between the slow decomposition of C_{60} film and the fast recrystallization of molecular fragments within the same locality gives rise to the co-existence of graphene and C_{60} phases. Due to bending rigidity of graphene, the growth of quasi-freestanding graphene on C_{60} molecules takes place. A second stage decomposition of the buried C_{60} molecules results in the growth of bilayer graphene. The results obtained here are relevant for understanding the growth dynamics of single and bilayer graphene from the decomposition of C_{60}. In addition, incorporation of herteroatoms on the fullerene cage may lead to the formation of novel graphene architectures with tunable electronic properties via recrystallization of their fragments at high temperature. It also verifies that suspended graphene can grow over nanosized obstacles on the substrates when the inter-particle distance between these obstacles are sufficiently small (< 4 nm). Our findings indicate the possibility of using nanospacers on metal substrate to grow suspended, flat graphene as opposed to the corrugated graphene routinely obtained on metal.

4. Experimental Section

The experiments were performed in an ultrahigh vacuum (UHV) chamber with a base pressure of 2×10^{-10} mbar. A UHV STM unit (SPECS high-temperature STM 150 Aarhus) is employed for imaging and spectroscopy studies (Nanonis, SPECS Zurich SPM control system). The STM chamber is adjoined to a preparation chamber equipped with Knudsen cells (MBE-Komponenten, Germany) for the evaporation of C_{60}. During deposition, the substrate was held at room temperature. The deposition rate of C_{60} was calibrated by counting the coverage of the large-scale STM images with coverage below 1 monolayer (one layer of fully covered C_{60}). The clean Ru(0001) surface (Mateck) was prepared based on the previous report.[17] In addition to STM topographic images, the STS data are taken at 100 K to reduce the thermal noise. STS was performed using standard lock-in techniques to acquire *dI/dV* with a modulation voltage of 20–50 mV with a frequency of 2.0 kHz (Nanonis, SPECS Zurich SPM control system). The STS curve is an arithmetic average of values measured at equally spaced 40–100 points on graphene.

Supporting Information

Supporting Information is available from the Wiley Online Library or from the author.

small 2012,
DOI: 10.1002/smll.201201113

Acknowledgements

This work is supported by NRF-CRP project "Graphene and Related Materials and Devices" (R-143-000-360-281).

[1] K. S. Novoselov, A. K. Geim, S. V. Morozov, D. Jiang, Y. Zhang, S. V. Dubonos, I. V. Grigorieva, A. A. Firsov, *Science* **2004**, *306*, 666
[2] K. S. Novoselov, A. K. Geim, S. V. Morozov, D. Jiang, M. I. Katsnelson, I. V. Grigorieva, S. V. Dubonos, A. A. Firsov, *Nature* **2005**, *438*, 197.
[3] Y. B. Zhang, T. T. Tang, C. Girit, Z. Hao, M. C. Martin, A. Zettl, M. F. Crommie, Y. R. Shen, F. Wang, *Nature* **2009**, *459*, 820.
[4] A. H. Castro Neto, F. Guinea, N. M. R. Peres, K. S. Novoselov, A. K. Geim, *Rev. Mod. Phys.* **2009**, *81*, 109.
[5] C. Riedl, C. Coletti, T. Iwasaki, A. A. Zakharov, U. Starke, *Phys. Rev. Lett.* **2009**, *103*, 246804.
[6] A. Varykhalov, W. Gudat, O. Rader, *Adv. Mater.* **2010**, *22*, 3307.
[7] X. Du, I. Skachko, A. Barker, E. Y. Andrei, *Nat. Nanotechnol.* **2008**, *3*, 491.
[8] W. Z. Bao, F. Miao, Z. Chen, H. Zhang, W. Y. Jang, C. Dames, C. N. Lau, *Nat. Nanotechnol.* **2009**, *4*, 562.
[9] H. Zhang, Q. Fu, Y. Cui, D. L. Tan, X. H. Bao, *J. Phys. Chem. C* **2009**, *113*, 8296.
[10] S. Park, R. S. Ruoff, *Nat. Nanotechnol.* **2009**, *4*, 217.
[11] J. Z. Wang, K. K. Manga, Q. L. Bao, K. P. Loh, *J. Am. Chem. Soc.* **2011**, *133*, 8888.
[12] A. M. Shikin, D. Farias, K. H. Rieder, *Europhys. Lett.* **1998**, *44*, 44.
[13] A. M. Shikin, Y. S. Dedkov, V. K. Adamchuk, D. Farias, K. H. Rieder, *Surf. Sci.* **2000**, *452*, 1.
[14] S. V. Kusminskiy, D. K. Campbell, A. H. C. Neto, F. Guinea, *Phys. Rev. B* **2011**, *83*, 165405.
[15] J. Lu, A. H. C. Neto, K. P. Loh, *Nat. Commun.* **2012**, *3*, 823.
[16] G. Schull, R. Berndt, *Phys. Rev. Lett.* **2007**, *99*, 226105.
[17] J. Lu, P. S. E. Yeo, C. K. Gan, P. Wu, K. P. Loh, *Nat. Nanotechnol.* **2011**, *6*, 247.
[18] E. V. Rutkov, A. Y. Tontegode, M. M. Usufov, *Phys. Rev. Lett.* **1995**, *74*, 758.
[19] L. F. Yuan, J. L. Yang, H. Q. Wang, C. G. Zeng, Q. X. Li, B. Wang, J. G. Hou, Q. S. Zhu, D. M. Chen, *J. Am. Chem. Soc.* **2003**, *125*, 169.
[20] J. V. Barth, *Annu. Rev. Phys. Chem.* **2007**, *58*, 375.
[21] K. Kern, J. V. Barth, G. Costantini, *Nature* **2005**, *437*, 671.
[22] A. Chuvilin, E. Bichoutskaia, M. C. Gimenez-Lopez, T. W. Chamberlain, G. A. Rance, N. Kuganathan, J. Biskupek, U. Kaiser, A. N. Khlobystov, *Nat. Mater.* **2011**, *10*, 687.
[23] J. Lu, P. S. E. Yeo, Y. Zheng, Z. Y. Yang, Q. L. Bao, C. K. Gan, K. P. Loh, *Acs Nano* **2012**, *6*, 944
[24] M. Gyamfi, T. Eelbo, M. Wasniowska, R. Wiesendanger, *Phys. Rev. B* **2011**, *83*, 153418.
[25] Y. B. Zhang, V. W. Brar, F. Wang, C. Girit, Y. Yayon, M. Panlasigui, A. Zettl, M. F. Crommie, *Nat. Phys.* **2008**, *4*, 627.
[26] E. Hernandez, V. Meunier, B. W. Smith, R. Rurali, H. Terrones, M. B. Nardelli, M. Terrones, D. E. Luzzi, J. C. Charlier, *Nano Lett.* **2003**, *3*, 1037.
[27] M. Koshino, Y. Niimi, E. Nakamura, H. Kataura, T. Okazaki, K. Suenaga, S. Iijima, *Nat. Chem.* **2010**, *2*, 117.
[28] H. Hibino, S. Mizuno, H. Kageshima, M. Nagase, H. Yamaguchi, *Phys. Rev. B* **2009**, *80*, 085406.
[29] M. L. Bocquet, B. Wang, S. Marchini, S. Gunther, J. Wintterlin, *Phys. Chem. Chem. Phys.* **2008**, *10*, 3530.
[30] A. Fasolino, J. H. Los, M. I. Katsnelson, *Nat. Mater.* **2007**, *6*, 858.
[31] P. A. Gravil, M. Devel, P. Lambin, X. Bouju, C. Girard, A. A. Lucas, *Phys. Rev. B* **1996**, *53*, 1622.
[32] M. Neek-Amal, N. Abedpour, S. N. Rasuli, A. Naji, M. R. Ejtehadi, *Phys. Rev. E* **2010**, *82*, 051605.

Received: May 22, 2012
Published online: